sustainability

MDPI

Article

Recycling Untreated Coal Bottom Ash with Added Value for Mitigating Alkali–Silica Reaction in Concrete: A Sustainable Approach

Safeer Abbas [1], Uzair Arshad [1], Wasim Abbass [1], Moncef L. Nehdi [2,*] and Ali Ahmed [1]

[1] Civil Engineering Department, University of Engineering and Technology Lahore, Lahore 54890, Pakistan; safeer.abbas@uet.edu.pk (S.A.); uzairarshad64@gmail.com (U.A.); wabbass@uet.edu.pk (W.A.); ali@uet.edu.pk (A.A.)

[2] Department of Civil and Environmental Engineering, Western University, London, ON N6A 5B9, Canada

* Correspondence: mnehdi@uwo.ca; Tel.: +1-519-6612111 (ext. 88308)

Received: 30 November 2020; Accepted: 17 December 2020; Published: 19 December 2020

Abstract: Each year, about 730 million tons of bottom ash is generated in coal fired power plants worldwide. This by-product can be used as partial replacement for Portland cement, favoring resource conservation and sustainability. Substantial research has explored treated and processed coal bottom ash (CBA) for possible use in the construction industry. The present research explores using local untreated and raw CBA in mitigating the alkali–silica reaction (ASR) of reactive aggregates in concrete. Mortar bar specimens incorporating various proportions of untreated CBA were tested in accordance with ASTM C1260 up to 150 days. Strength activity index (SAI) and thermal analysis were used to assess the pozzolanic activity of CBA. Specimens incorporating 20% CBA achieved SAI greater than 75%, indicating pozzolanic activity. Mixtures incorporating CBA had decreased ASR expansion. Incorporating 20% CBA in mixtures yielded 28-day ASR expansion of less than the ASTM C1260 limit value of 0.20%. Scanning electron microscopy depicted ASR induced microcracks in control specimens, while specimens incorporating CBA exhibited no microcracking. Moreover, low calcium-to-silica ratio and reduced alkali content were observed in specimens incorporating CBA owing to alkali dilution and absorption, consequently decreasing ASR expansion. The toxicity characteristics of CBA indicated the presence of heavy metals below the US-EPA limits. Therefore, using local untreated CBA in concrete as partial replacement for Portland cement can be a non-hazardous alternative for reducing the environmental overburden of cement production and CBA disposal, with the added benefit of mitigating ASR expansion and its associated costly damage, leading to sustainable infrastructure.

Keywords: coal; bottom ash; reactive aggregate; concrete; durability; alkali–silica reaction; expansion; toxicity; sustainable infrastructure

1. Introduction

Alkali–silica reaction (ASR) is a common deterioration process in concrete structures incorporating reactive aggregates. Alkalis present in the pore solution react with siliceous phases in reactive aggregates and produce alkali–silica gel. This ASR gel absorbs moisture and swells, leading to distress and cracking, possibly compromising the structural integrity and durability of concrete structures [1–3]. It has been posited that the availability of calcium ions is important for preserving desirable alkalinity levels in the pore solution [4]. Various reactive aggregates such as Spratt, opaline silica, strained quartz, cristobalite, chalcedony, volcanic glasses and ferronickel slag were found to accelerate ASR [5,6]. Other factors that cause adverse ASR in concrete structures include the presence of moisture, type of alkali constituents and exposure to higher temperature [1].

Various structures around the world have incurred ASR damage. For example, several bridges in Japan [7], concrete pavements and bridges in the United States and Canada [8,9], fly-over piers in Poland [10], the Elgeseter bridge in Norway [11] and several hydraulic structures in Pakistan [12] were severely damaged by ASR. It was reported that routine operations of various dam structures such as sluice gates may be disrupted due to misalignment induced by ASR expansion [13,14]. Furthermore, cracking initiates when ASR expansion exceeds the tensile capacity of concrete. This accelerates the intrusion of aggressive species into concrete, promoting other damage mechanisms such as reinforcing steel corrosion, sulphate attack and damage by freezing and thawing cycles.

Ordinary Portland cement (OPC) concrete is the most consumed commodity after water. It depletes natural resources, consumes substantial energy in its production, and releases about 8% of the global CO_2 emissions [15,16]. Supplementary cementitious materials (SCM) such as silica fume, fly ash, metakaolin, ground granulated blast furnace slag, rice husk ash, and sugarcane bagasse ash can be used as partial replacement for OPC, decreasing its carbon footprint and limiting the consumption of virgin natural resources. SCMs can be used for mitigating ASR expansion by decreasing permeability and the alkali content in the pore solution through alkali binding [17]. SCMs having low alkalis and calcium oxide contents were found to be more effective in controlling ASR [18]. Saha and Sarker [19] reported approximately 65% reduction in ASR expansion due to the incorporation of 20% fly ash. Similarly, Abbas et al. [20] reported that using rice husk ash as partial replacement for OPC can control ASR expansion and the associated cracking. In another study, Abbas et al. [21] reported 20% and 40% reduction in ASR expansion due to the addition of 10% and 40% of sugarcane bagasse ash as partial OPC replacement, respectively.

Coal bottom ash (CBA) is the deposit residue left after the combustion of coal in thermal power plants. Coal fired power plants contribute approximately 38% of the world's electricity and generate enormous amounts of coal combustion waste [22,23]. CBA is collected from the bottom of coal combustion boilers in power plants, with annual world production of about 730 million tons [24,25]. For instance, India produces 110 million tons of CBA annually from 70 power plants [26], while Thailand and Turkey generate 3.5 and 13 million tons of CBA each year, respectively [27,28]. CBA may contain toxic components that can harm the surrounding environment in open landfill deposition, threatening human health and disturbing ecosystems. In the United States, around 12 million tons of CBA is used annually in various construction activities [29]. The chemical, physical and mechanical properties of CBA depend on the nature of the used coal and the combustion process, along with the boiler conditions [24].

Various studies have been conducted to explore the mechanical properties of concrete mixtures incorporating treated CBA. For instance, it was reported that using CBA as sand replacement increased the concrete compressive and flexural strengths and decreased its shrinkage strains [30–33]. Oruji et al. [34] studied the utilization of ultrafine coal bottom ash as partial cement replacement for the mitigation of alkali–silica reaction in concrete. The studied dosage of ultrafine coal ash was 9%, 23%, 33% and 41%, while maintaining the water-to-binder ratio at 0.55. It was observed that on replacing 9% cement with ultrafine coal ash, the compressive strength of concrete increased by 11% at 28 days compared to that of the control specimens. Further, it was reported that the ASR expansion was decreased at all ultrafine coal ash dosages. Specimens were tested up to 28 days [34]. Gooi et al. [35] reported the effect of partial substitution of aggregates and cement in concrete by coal bottom ash (CBA) on the compressive strength based on existing literature. It was reported that using CBA in concrete makes it more porous. Large variation in the reported results was observed due to various types of bottom ash and its treatment procedures. Moreover, it was reported that the loss on ignition (LOI) had insignificant effect on the concrete compressive strength at later ages [35]. Muthusamy et al. [36] investigated the effect of CBA content as partial replacement for sand on the workability and compressive strength of concrete. Four replacement levels (10%, 20%, 30% and 40%) were investigated with the water-to-cement ratio maintained at 0.325. A reduction in workability and compressive strength was reported for mixtures incorporating CBA compared to that of the control

mixture. Similarly, Arun et al. [37] investigated the effect of variable grinding bottom ash (i.e., for 1 h, 2 h and 4 h) on the compressive strength of concrete. It was observed that reducing the size of bottom ash particles, increased the compressive strength and decreased porosity [37].

The global energy requirement has increased over the years due to population growth. It is estimated that around 47% of electricity would be generated through coal combustion by year 2030 [38]. Pakistan has very large reserves of coal, which can generate electricity of more than 100,000 MW which resulted in enormous amounts of coal ash. In Pakistan, both wet and dry coal ash deposition systems are being implemented in various power plants and dumped in open landfills and disposal ponds [39]. This open landfilling practice threatens the surrounding physical, biological and social environments [40]. Therefore, it is of utmost importance to investigate the potential applications of local coal bottom ash (CBA) in the construction industry for attaining sustainable development goals.

The physical and chemical properties of CBA are highly dependent on the source of the parent coal and its geographical locations. Further, the pre-processing of CBA to beneficiate it for use as a construction material involve substantial costs and labor. Therefore, there is need to examine the feasibility of using local untreated CBA in construction activities for achieving sustainable civil infrastructures. Moreover, very scant literature exists on the use of untreated local CBA for controlling ASR damage in concrete structures.

Therefore, this study investigates the physical and chemical properties of local untreated CBA, its concentration of heavy metals and compares the results with previous studies (CBA produced in different countries), the pozzolanic activity of untreated local CBA and its possible role in controlling ASR damage in concrete. The study of the microstructural features of mixtures incorporating local CBA and exposed to ASR conducive conditions adds novelty to this research. Furthermore, the effect of ASR conditions (specimens placed in NaOH solution at 80 °C) on mechanical properties (compressive and flexural strength) up to 150 days were investigated. The results should allow construction stakeholders to efficiently use untreated local CBA currently disposed in landfills in added value construction applications, leading to eco-friendly, economical and sustainable construction, with the further benefit of mitigating ASR.

2. Materials and Methods

2.1. Materials

Aggregates were procured from a local crusher plant, washed with clean water, then dried in a laboratory oven. Afterwards, aggregates were crushed and sieved to various size fractions, then combined in various proportions in accordance with ASTM C1260 [41]. CBA was obtained from a local thermal power plant and sieved through sieve # 200. CBA was black in color, showing substantial unburnt content. Commercially available OPC was also used. Various CBA dosages (10%, 20%, 30% and 40% by cement mass) were investigated. The concrete mixture design used for preparing the test specimens was 1:2.25 cement-to-aggregate ratio and 0.47 water-to-cement ratio (w/c), as per ASTM C1260 [41]. Table 1 shows the mixture proportions for prepared test specimens.

Table 1. Mixture proportions.

Cement (kg/m^3)	Aggregate (kg/m^3)	Water (kg/m^3)
724	1629	340

2.2. Tests on Raw Materials

The chemical composition of cement, coal bottom ash (CBA) and aggregates were examined using X-ray fluorescence (XRF) and X-ray diffraction (XRD) analysis. Scanning electron microscopy (SEM) and energy dispersive X-ray (EDX) analysis were carried out to examine the micro-structure of cement and CBA. The fineness of cement and CBA were determined using ASTM C184 [42] and ASTM

C204 [43]. The specific gravity of raw materials was calculated according to ASTM C188 [44]. Moreover, autoclave expansion of OPC was determined in accordance with ASTM C151 [45]. Various tests including crushing, abrasion resistance, impact resistance, specific gravity, bulk density and water absorption were performed on coarse aggregates. The mineralogical composition of the aggregates was assessed via petrographic analysis, as per ASTM C295 [46] using grains mounted on thin sections and polished using different size abrasive powders. A petrographic microscope at both cross and plan light with low and high magnification power was used. The toxicity characteristics of CBA were examined on approximately 50 g of dried powder per the toxicity characteristics leaching procedure (TCLP) [47], which is commonly used for evaluating the hazardous nature of waste materials [48].

2.3. Fresh Properties of Mixtures Incorporating CBA

Various tests on the fresh properties of mixtures incorporating cement, CBA and aggregates were performed. Consistency and setting time of mixtures were measured using ASTM C187 [49] and ASTM C191 [50], respectively. Flowability of mixtures was measured using the flow table test in accordance with ASTM C1437 [51].

2.4. Cube and Prism Specimens

Cubic ($50 \times 50 \times 50$ mm) and prismatic ($40 \times 40 \times 160$ mm) specimens were prepared. Four identical specimens were made for each mixture and testing age. Specimens were cast in two layers on a vibratory table and demolded after 24 h, then placed in curing water until testing. Compressive and flexural strength tests were performed at desired ages as per ASTM C109 [52] and ASTM C348 [53], respectively. The loading rate for compression and flexural testing was 1000 N/s and 2600 N/s, respectively. Strength activity index (SAI) was calculated in accordance with ASTM C311 [54]. Moreover, specimens were placed in 1 N sodium hydroxide (NaOH) solution at 80 ± 3 °C to examine the effects of ASR on the compressive and flexural strengths. The porosity of concrete cube specimens incorporating various CBA dosages was determined using the volume of permeable voids test as per ASTM C642 [55]. The density of specimens was determined via measuring the mass divided by the respective volume. Thermal analysis on concrete specimens incorporating various proportions of untreated CBA was also conducted using SQT Q600 TA instrument. Powder samples were heated to 1200 °C at a heating rate of 20 °C/min for measuring the mass change and heat flow.

2.5. Mortar Bars

Five mortar bar specimens ($25 \times 25 \times 285$ mm) were made for each mixture to measure ASR expansion in accordance with ASTM C1260 [41]. Specimens were covered with plastic sheets to prevent moisture loss. After 24 h, specimens were demolded, and their initial length was measured using a calibrated digital length comparator as per ASTM C490 [56]. Specimens were then placed in water at 80 ± 3 °C until 24 h and their length was measured, before being placed in a NaOH solution at 80 ± 3 °C. Change in length for each specimen was measured at 3, 7, 14, 21, 28, 42, 56, 90, 120 and 150 days. Each specimen was visually inspected for surface distress and cracking. Microstructural features of small fragments extracted from selected specimens were also studied using a Ziess scanning electron microscope (SEM). Furthermore, energy dispersive X-ray (EDX) analysis with accelerating voltage of 20 keV, was used to obtain elemental composition.

3. Results and Discussion

3.1. Characterization of Raw Materials

SEM images of OPC and untreated CBA showed irregular comparable size particles of varying dimensions (Figure 1). CBA particles exhibited uneven and porous spongy structure (Figure 2) unlike the spherical fly ash particles. The average pore size in untreated CBA particles was about

8 µm (Figure 2). Similar observations regarding the SEM images of CBA were reported in previous studies [57,58].

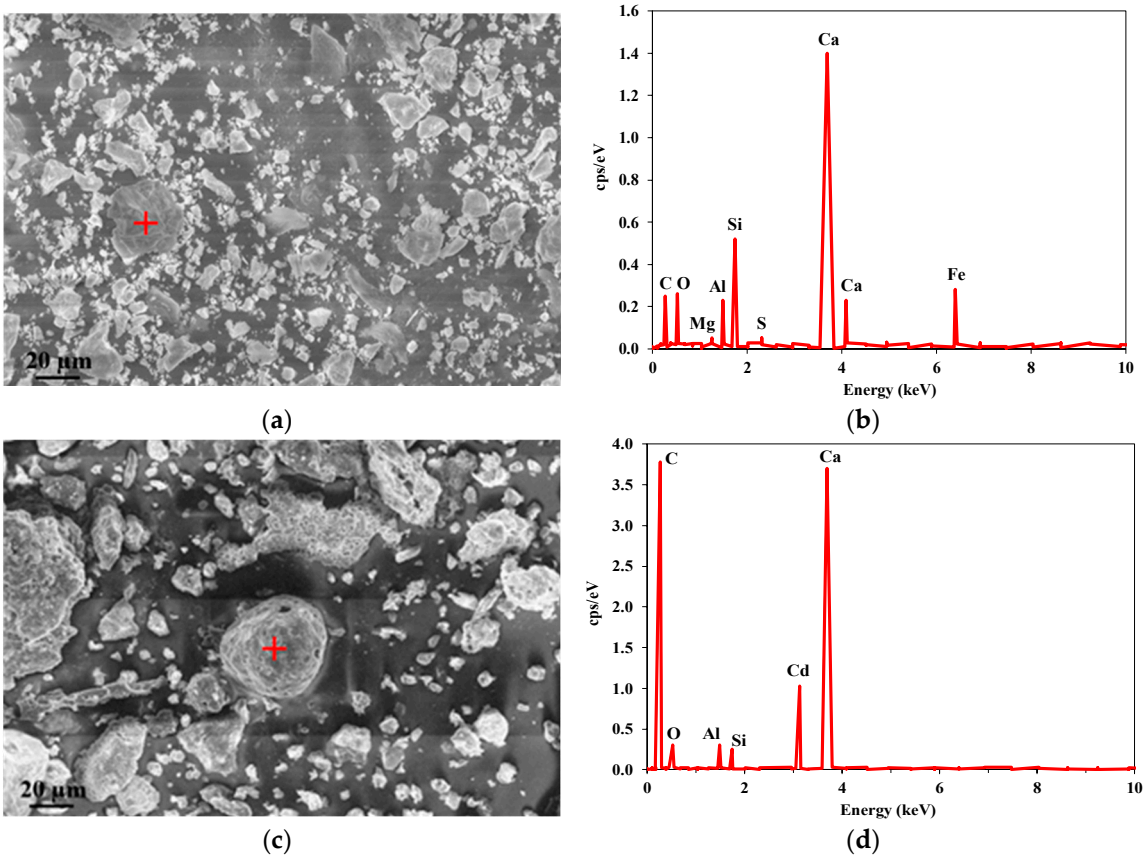

Figure 1. SEM and EDX analysis of cement and coal bottom ash. (**a**) SEM image of cement, (**b**) EDX of cement (+), (**c**) SEM image of coal bottom ash, and (**d**) EDX of coal bottom ash (+).

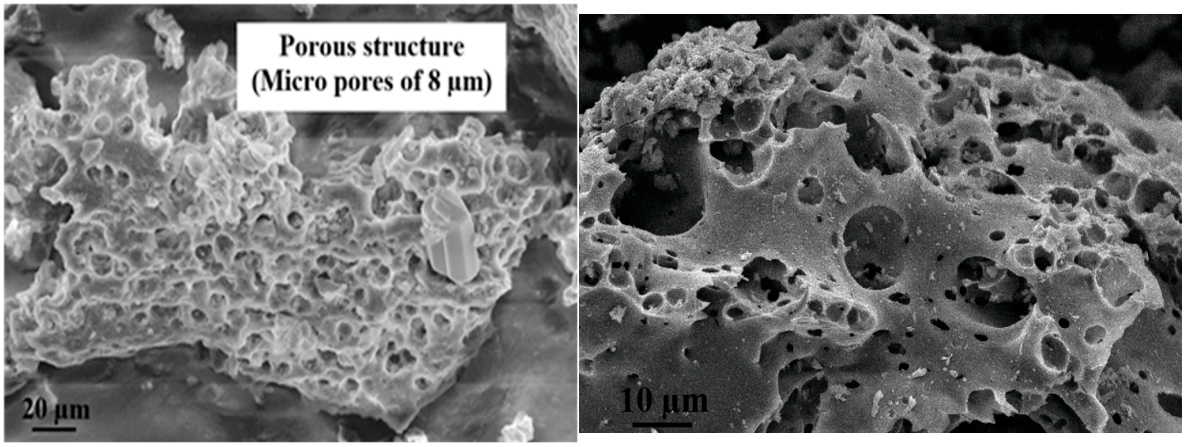

Figure 2. Porous structure of coal bottom ash.

EDX analysis showed that the major constituents of untreated CBA were carbon (C), silicon (Si), calcium (Ca) and aluminum (Al), with traces of cadmium (Cd) (Figure 1b). Table 2 shows the chemical analysis of OPC and CBA. The combined sum of SiO_2, Al_2O_3 and Fe_2O_3 for CBA was 49.5%, which is comparable to findings of previous study [59]. The CBA loss on ignition (LOI) was 10.85%, also in agreement with previous findings [60]. For instance, Kim [61] and Targan et al. [62,63] reported LOI greater than 10% for CBA. Higher LOI of SCMs usually may cause higher water demand, segregation

and discoloration of concrete mixtures, and decrease in compressive strength [27,64]. XRD analysis of OPC identified di-calcium silicate (C_2S), tri-calcium silicate (C_3S) and gypsum. Peaks of quartz and mullite were also observed in XRD analysis of CBA (Figure 3).

Table 2. Chemical properties of cement and coal bottom ash.

Constituents	CaO	MgO	SiO_2	SO_3	Al_2O_3	Fe_2O_3	K_2O	Na_2O	LOI
Cement *	62.08	1.96	20.85	2.49	4.88	3.21	0.74	0.10	2.78
Coal bottom ash *	7.65	0.51	33.85	4.88	11.20	4.75	0.52	0.13	10.85
Kim (2015) [61]	0.99	1.25	45.74	-	25.33	6.86	3.71	0.70	12.60
Kurama and Kaya (2008) [28]	4.69	-	54.50	-	15.40	11.16	-	-	8.90
Siddique (2013) [65]	1.58	1.19	57.56	0.02	21.58	8.56	1.08	0.14	5.80
Targan et al. (2002) [62]	17.57	1.52	42.39	2.34	21.35	6.41	1.11	-	10.17
Singh and Siddique (2014) [66]	4.17	0.82	47.53	1.00	20.69	5.99	0.76	0.33	0.89
Oruji et al. (2017) [67]	9.50	1.60	58.70	0.40	20.10	6.20	1.00	0.10	0.80
Jaturapitakkul and Cheerarot (2003) [57]	11.48	3.47	46.02	1.52	22.31	10.64	3.47	0.07	2.72
Hashemi et al. (2018) [23]	4.19	1.24	50.49	0.10	27.56	10.93	0.82	0.57	1.11
Cheriaf et al. (1999) [68]	0.80	0.60	56.00	0.10	26.70	5.80	2.60	0.20	4.60
Rafieizonooz et al. (2016) [22]	8.70	0.96	45.30	0.35	18.10	19.84	2.48	-	-
Andrade et al. (2009) [69]	0.80	0.60	56.00	0.10	26.70	5.80	2.60	0.20	4.60
Fly ash (FA) **	5.11	2.15	50.77	1.20	26.65	10.06	0.61	0.77	1.08

* Present study; ** Oruji et al. [34].

Table 3 shows the concentration of heavy metals in CBA. The contents of lead (Pb), zinc (Zn), copper (Cu), Nickel (Ni) and chromium (Cr) were 18, 60, 23, 27 and 18 ppm, respectively. These values are within limits [70–74], indicating non-hazardous classification of CBA. The concentration of heavy metals in CBA was less than corresponding values for CBA produced elsewhere (Table 3). For instance, the concentration of Cr was 145 ppm and 134 ppm in CBA generated in India and Spain, respectively, which is higher than that in the present study (43 ppm). Similarly, Pb was 143 ppm and 176 ppm in coal ash produced in Greece [75] and the United Kingdom [76], respectively, which is higher than that in the present study (35 ppm). Indeed, the used CBA had heavy metal concentrations within the limits of heavily polluted sediments (50, 200 and 50 ppm for Cu, Zn and Ni, respectively) [77]. Table 3 shows the concentration of heavy metals in concrete mixtures incorporating various CBA dosages. The concentration of heavy metals (Pb, Zn, Cu, Ni and Cr) in concrete mixtures incorporating 10% and 40% of CBA were within allowable limits.

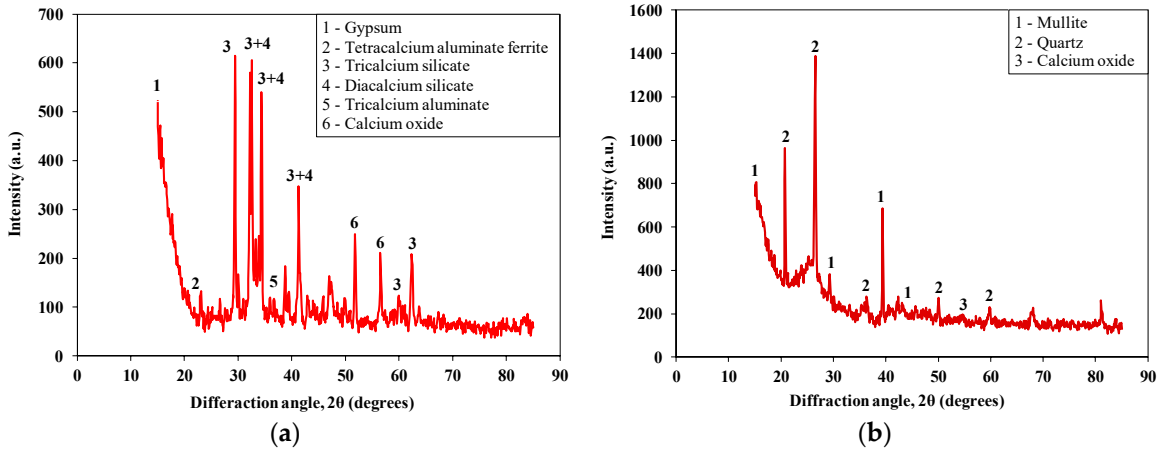

Figure 3. XRD patterns of raw materials using X-ray diffractometer (D8 DISCOVER Bruker). (**a**) XRD pattern of cement, and (**b**) XRD pattern of coal bottom ash.

Table 3. Concentration of heavy metals in used coal bottom ash (CBA) and its comparison with previous studies.

Region	Materials	Heavy Metals (ppm)				
		Lead (Pb)	Zinc (Zn)	Copper (Cu)	Nickel (Ni)	Chromium (Cr)
Pakistan *	Coal bottom ash	18	60	23	27	18
	CBA0	35	80	38	26	50
	CBA10	34	94	32	36	36
	CBA40	35	96	34	36	42
Macedonia [78]	Coal ash	50	191	80	68	114
Spain [79]		52	221	72	88	134
Greece [75]		143	59	63	-	-
United Kingdom [76]		176	-	-	-	-
India [80]		54	69	83	56	145
South Africa [81]		10	34	103	-	-
Poland [82]	Fly ash	44	120	38	41	64
Tharaniyil (2013) [83]		111	110	239	65	124
Finland [84]	Fly ash	25	72	34	50	35
	Limit for earth construction agent	300	200	400	-	400
USEPA [47,70–72]	-	300	2800	1500	-	1200
	Sludge	840	-	4300	420	3000
EUR, 2003 [74]	Hazardous waste	50	200	100	40	70
Hassaan et al. (2016) [77]	Sediment quality (Heavily polluted)	-	>200	>50	>50	-

* Present study; CBA0 = concrete mixture without coal bottom ash; CBA10 = concrete mixture with 10% of coal bottom ash; CBA40 = concrete mixture with 40% of coal bottom ash.

Table 4 shows physical properties of CBA and OPC. The specific gravity and unit weight of CBA were lower than that of OPC. The fineness of CBA and cement were 4355 cm^2/g and 3015 cm^2/g, respectively. Autoclave expansion of OPC was 0.10%, less than the ASTM C1260 limit (i.e., 0.2%). Therefore, the used OPC is suitable for accessing ASR. Physical properties of aggregates are shown in Table 5 and were within specified limits of ASTM standards. The impact and crushing values of aggregates were 22.31% and 24.58%, respectively. Table 5 also shows that aggregates were rich in silica content (77%), with presence of magnesium oxide (MgO), calcium oxide (CaO), ferric oxide (Fe_2O_3) and alumina (Al_2O_3).

Table 4. Physical properties of coal bottom ash and cement.

Properties	Coal Bottom Ash	Cement	Limits for Cement	Standards
Specific gravity	2.35	3.12	3.10—3.25	ASTM C188
Fineness (Passing 200 sieve) (%)	>95	95	>90	ASTM C204
Blaine fineness (cm^2/g)	4355	3015	>2250	ASTM C184
Unit weight (kg/m^3)	364	1545	–	–
Autoclave expansion (%)	-	0.10	0.20 *	ASTM C151
Standard consistency (%)	-	25.5	–	ASTM C187
Initial setting time (Minutes)	210	170	>45	ASTM C191
Final setting time (Minutes)	335	295	<375	ASTM C191

* For use in accelerated mortar bar test according to ASTM C1260. For mixture incorporating 20% of CBA.

Table 5. Physical and chemical properties of aggregates.

Properties	Tests	Results
Physical	Voids content (%)	40.71
	Bulk density (kg/m^3)	1448.00
	Specific gravity	2.60
	Water absorption (%)	2.20
	Impact value (%)	22.31
	Crushing value (%)	24.58
Chemical	Calcium oxide (%)	3.60
	Magnesium oxide (%)	2.40
	Loss on ignition (%)	7.80
	Silica (%)	77.20
	Alkali metals (%)	0.40
	Ferric oxide (%)	4.38
	Alumina (%)	4.02

Petrographic analysis revealed that the aggregates were comprised of sandstone (85%), siltstone (4%) and shale (11%) (Table 6). Sandstone was fine to medium grained (0.10 to 0.60 mm) and grayish to brown in color. This sub-group consisted predominantly of quartz and feldspar with a minor amount of clays, lithics, mafic phases (amphibole, pyroxene and mica) and ores. Quartz occurred either as discrete grains (78%) or as part of lithics (granite and quartzite), which formed the dominant phase of the aggregate, showing angular, subangular to sub-spherical shape. About 35% of the quartz grains exhibited wavy extinction or showed poly-crystalline structure, indicating strained and deformed nature. Fine to medium-grained feldspar occurred dominantly as K-feldspar with minor amount of plagioclase. Plagioclase was characterized by a diagnostic twining pattern. Both K-feldspar and plagioclase collectively formed 9% of the aggregate in the form of discrete grains. K-feldspar also occurred as part of granitic fragments and showed partial alteration to clays. Ferruginous clays occurred as part matrix around grains and constituted around 6% of clays. Lithics occurred in the form of quartzite and granite, while amphibole, pyroxene and mica constituted the mafic phases. Opaque minerals were dominantly magnetite/hematite, which formed up to 1% of the sub-group.

Table 6. Petrographic analysis of aggregates.

Rock Types		Percentage (%)
Sandstone (85%)	Quartz (monocrystalline)	43
	Quartz * (Polycrystalline)	35
	Plagioclase	9
	Ferruginous clays *	6
	Quartzite	3
	Amphibole	1
	Opaque minerals	3
Siltstone (4%)	Quartz (monocrystalline)	69
	Quartz * (Polycrystalline)	9
	Feldspar	19
	Ferruginous clays	1
	Amphibole	1
	Ores	1
Shale * (11%)	Ferruginous clays *	75
	Quartz *	25

* Deleterious components.

Siltstone was fine grained with grayish color. It consisted predominantly of quartz and feldspar with a minor amount of clays, lithics, mafic phases (amphibole, pyroxene and mica) and ores. Quartz either occurred as discrete grains (78%), which formed the dominant phase of the aggregate with

sub-angular to sub-rounded and subspherical shape. About 9% of the quartz grains exhibited undulose extinction or showed poly-crystalline nature, which indicates its strained/deformed character. Fine silt-size feldspar occurred as K-feldspar, showing alteration to clays. Very few plagioclase grains were also observed. Feldspar constituted about 19% of the aggregate in the form of discrete grains, mostly altered to clays. Ferruginous clays occurred as part matrix around grains and constituted around 1% of fragments. Forming 1% of the siltstone sub-group, the mafic phases included amphibole, pyroxene and mica. Opaque phases were dominantly magnetite/hematite and occurred as minor phases.

Shale was reddish brown and consisted of clay size (>1/256 mm) ferruginous clays and silt size (≥1/256 to 1/16 mm) grains of quartz. Clays and quartz constituted about 75% and 25% by volume, respectively. It can be argued that the aggregate consisted of strained-quartz (deformed) and polycrystalline quartz, which can potentially cause ASR. Furthermore, siltstone and shales/phyllite fragments within the aggregates were present, which are also ASR deleterious.

3.2. Flow of Mixtures Incorporating Coal Bottom Ash

Table 7 shows the flow of mixtures incorporating various dosages of CBA. Flow of the control mixture without CBA was 113 mm but decreased due to incorporation of CBA. For instance, 8% decrease in flow was observed for the mixture incorporating 30% CBA. High water absorption of CBA compared to that of OPC is responsible for the reduction of flow properties. Additionally, the used CBA had rougher and more irregular particles, which created friction and restricted flow, as observed by others [33,63,85]. Aydin [86] reported 7% decrease in flow for mixtures incorporating CBA compared to that of control mixtures without CBA. Jaturapitakkul and Cheerarot [57] also reported 7% decrease in flow for mixture incorporating 10% CBA compared to that of the control mixture. The water demand increased for achieving desired flow due to the porous nature of CBA [57]. Additionally, 17% decrease in workability was observed in previous study for mixture incorporating 20% of ground CBA [87]. To mitigate the reduction of flow of mixtures incorporating CBA, superplasticizers can be used. Additionally, the grinding of CBA may decrease its porosity and angularity, leading to increased flow properties.

Table 7. Flow results of mixtures incorporating coal bottom ash.

Mixtures	CBA0	CBA10	CBA10	CBA10	CBA10
Flow (mm)	113	109	107	104	101

The standard consistency of cement paste was 25.5%. The initial and final setting times of the control OPC paste were 170 and 295 min, respectively. Incorporating CBA in concrete mixtures increased the setting time. For instance, mixtures incorporating 20% CBA had initial and final setting times of 210 and 335 min, respectively. This increase in setting times can be attributed to cement dilution as reported in previous studies [27,57].

3.3. Porosity and Density

Figure 4 shows the volume of permeable voids (VPV) for mixtures incorporating various proportions of CBA at 28 and 56 days. The VPV increased for mixtures with higher proportions of CBA. For example, VPV of the control mixture without CBA was 6.82% at 28 days and increased to 7.74%, 7.94%, 8.50% and 10.94% for mixtures incorporating 10%, 20%, 30% and 40% of CBA, respectively. The microstructure of OPC was dense, compact and non-porous (Figure 1a). Conversely, CBA had a porous morphology (Figure 2). Thus, increased VPV using CBA as partial replacement for OPC is mainly attributed to the CBA porous nature. Reduction in VPV was observed at 56 days (Figure 4a). For instance, the VPV for the mixture incorporating 10% of CBA was 6.40% and 7.74% at 56 and 28 days, respectively. This reduction in porosity at later age is attributed to the progress of hydration and pozzolanic reactions and formation of additional calcium silicate hydrates (CSH).

Dry densities of mixtures incorporating various proportions of CBA at 28 and 56 days are shown in Figure 4b. Control specimens without CBA had density of 2353 kg/m^3 at 28 days. A decrease in density was observed for specimens incorporating CBA. For instance, specimens incorporating 30% CBA had 7% decrease in density at 28 days compared to that of the control specimens without CBA. Maximum decrease in density was observed for the mixture incorporating 40% CBA due to the lower specific gravity of CBA. Similar decrease in density due to incorporation of CBA was reported in previous study [88]. At 56 days, the density of tested specimens was increased due to the continuous hydration process and formation of secondary CSH (Figure 4b).

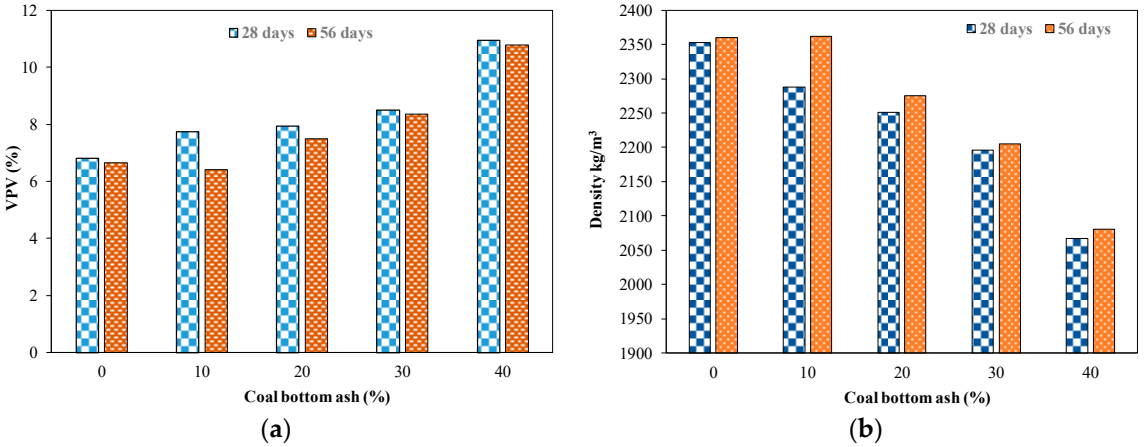

Figure 4. Volume of permeable voids (VPV) and density results at various ages. (**a**) VPV for mixtures with CBA, and (**b**) density for mixtures with CBA.

3.4. Thermal Analysis

Figure 5 shows differential scanning calorimetry (DSC) and thermogravimetric analysis (TGA) of CBA. Sharp peaks in the DSC curve indicate heterogenous combustion, while relatively flat curve indicates homogenous combustion [89]. The DSC curve of the untreated CBA showed an initial endothermic peak at around 73 °C due to the loss of physically bound water [90]. Two smaller endothermic peaks were observed at around 135 and 390 °C. An exothermic peak was also observed at around 579 °C, indicating the presence of quartz. Quartz inversion was evident in the temperature range of 530 to 580 °C [90]. Similarly, Marinkovic et al. [91] also reported exothermic peak at 469 °C for CBA related to unburnt carbon particles. An endothermic peak was observed at 769 °C, which may be attributed to the presence of carbonates. Similar findings were also reported in previous study [91]. The TGA curve (Figure 5) showed total mass loss of about 64%. Maximum mass loss was observed in the range of 495 to 930 °C. After 930 °C, the CBA showed thermogravimetric stable behavior. Santos et al. [92] reported loss of humidity up to 100 °C, loss of hydration products from 100 to 340 °C, decomposition of calcium carbonate ($CaCO_3$) in the range of 430 to 750 °C and above 750 °C major mass loss related to high ash content in coal fly ash [92].

Figure 6 illustrates thermal analysis (DSC and TGA) results for concrete mixtures incorporating CBA. DSC curves (Figure 6a) for control specimens and specimens incorporating CBA were comparable, though exhibited different heat flow values at similar temperature, as previously observed by Saha and Sarker [19]. For control specimens without CBA, an initial endothermic peak was observed at around 93 °C, which is related to the evaporation of water in micropores. Other endothermic peaks were observed at around 445 and 740 °C. These peaks are related to the decomposition of portlandite (CH) and calcium carbonates ($CaCO_3$), respectively [20,21,93,94]. For specimens incorporating 10% CBA, endothermic peaks were observed at approximately 98, 457 and 740 °C, similar to control specimens without CBA. However, specimens incorporating 40% CBA showed an initial endothermic peak at around 61 °C. Other smaller peaks were observed at around 238, 473 and 735 °C for specimens incorporating 40% CBA.

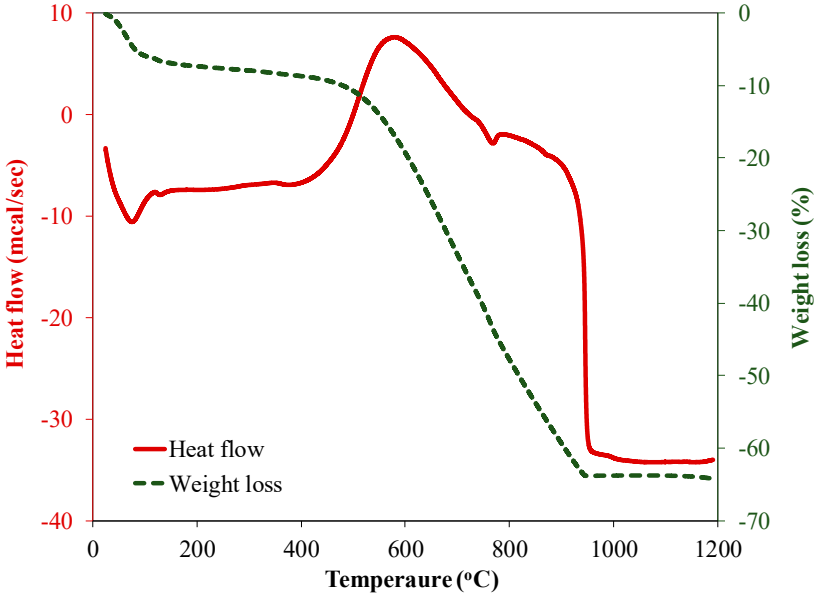

Figure 5. Thermal analysis of untreated coal bottom ash.

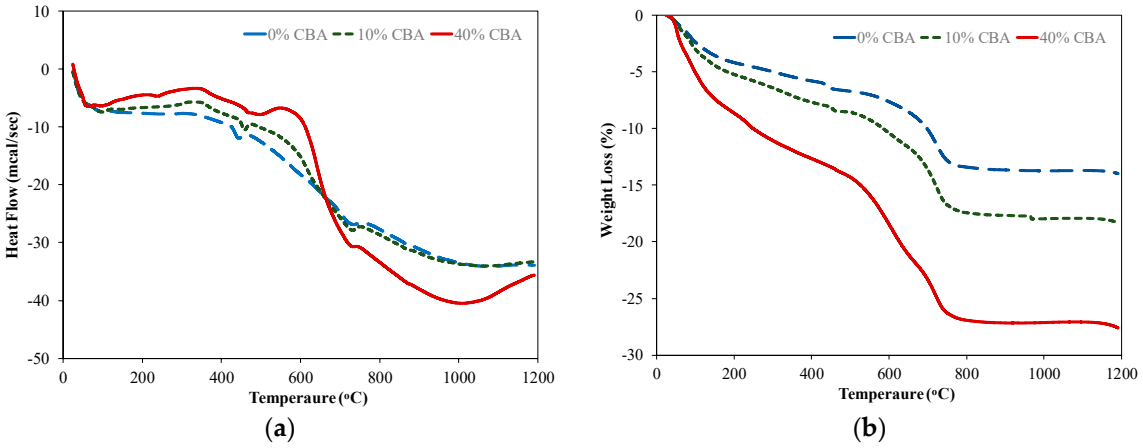

Figure 6. Thermal analysis of specimens incorporating various proportions of CBA. (**a**) Heat flow, and (**b**) Weight loss.

TGA curves of specimens incorporating various proportions of CBA can be divided into four zones (Figure 6b): 45 to 160 °C, 161 to 510 °C, 511 to 770 °C and 771 to 1200 °C. Approximately, 3.5%, 4.5% and 7.5% of mass loss was observed for specimens without CBA, 10% CBA and 40% CBA, respectively, in the temperature range of 45 to 160 °C. Similarly, mass loss of 2.5%, 3.5% and 6.5% was observed from 161 to 510 °C for specimens without CBA, 10% CBA and 40% CBA, respectively. More mass loss was observed from 511 to 770 °C for all specimens. Approximately, 6.5%, 8.5% and 12.5% mass loss was observed for specimens without CBA, 10% CBA and 40% CBA, respectively, in that temperature range. Beyond 770 °C, constant mass loss was observed for all tested specimens. Mass loss increased for specimens incorporating higher CBA dosage. For example, mass loss of 13%, 17% and 27% at 1200 °C was recorded for control specimens, and specimens with 10% and 40% CBA, respectively. This mass loss is attributed to loss of adsorbed water in micropores, decomposition of hydrated compounds, disintegration of $CaCO_3$ and burning of organic matter [23,95]. Presence of CH can act as a cation exchanging and essential component for the development of ASR gel and associated damage [4,67,96]. Further, it was also observed that the increased amount of CH can contribute towards reduction in strength development by enabling ASR gel to expand the surrounding matrix [4]. The removal of CH from the system can mitigate expansion [4,97]. The CH content for different samples

incorporating coal ash was determined through mass loss of dehydroxylated between 400 and 600 °C using Equation (1) [98].

$$CH = \frac{74}{18}\frac{M_{400} - M_{600}}{M_c} \quad (1)$$

where, M_{400} and M_{600} are the mass loss at temperatures of 400 and 600 °C, respectively. M_c is the initial anhydrous cement mass in grams. The values 74 and 18 are the molar mass ratio of $Ca(OH)_2$ and H_2O [98]. It has been observed that specimens incorporating local untreated CBA (i.e., 10% and 40%) exhibited lower *CH* content than the control specimen without CBA. Control specimens had higher *CH* content of 12% with respect to 9% and 7% for specimens incorporating 10% and 40% of CBA, respectively. Similar findings were reported in previous studies [99,100].

3.5. Effect of CBA on Compressive and Flexural Strength

The compressive strength of mixtures incorporating various proportions of untreated CBA was determined on four identical cube specimens at each testing date. Average results are reported in Figure 7, showing coefficient of variance less than 2.50%. The compressive strength ($f'c$) increased with longer curing time, as expected, due to continuing hydration process [21]. For instance, for control specimens, $f'c$ was around 33% higher at 56 days compared to that at 14 days. It increased from 29 MPa at 28 d to 42 MPa at 150 d for control specimens. The mixture incorporating 10% CBA had comparable 28 d $f'c$ (28 MPa) to that of the control specimens without CBA (29 MPa). Beyond 28 days, $f'c$ of the mixture incorporating 10% CBA was higher than that of the control mixture without CBA. For instance, $f'c$ for specimens incorporating 10% CBA at 56, 90 and 150 days was 13%, 17% and 20%, higher than that of control specimens without CBA, respectively. This increase is mainly related to delayed pozzolanic reactions of CBA leading to formation of more calcium silicate hydrates (CSH). It was reported that the consumption of CH was higher at later ages (60% at 90 days) compared to early ages (5% at 7 days) [68]. The used CBA had low calcium content, which did not promote contribution to early age $f'c$. On the other hand, high amorphous silica content in CBA contributed to secondary CSH through pozzolanic reactions, leading to reduced porosity and increased $f'c$ beyond 28 days, as observed in previous study [19]. Formation of stable secondary CSH depends on the shape, size, orientation, distribution, volume and topology of pozzolanic material particles [28]. For specimens incorporating 20% of untreated CBA, the 28 d $f'c$ was lower than that of the control specimens. However, at later ages (56, 90, 120 and 150 days), $f'c$ for specimens incorporating 20% of CBA was comparable to that of the control specimens (Figure 7).

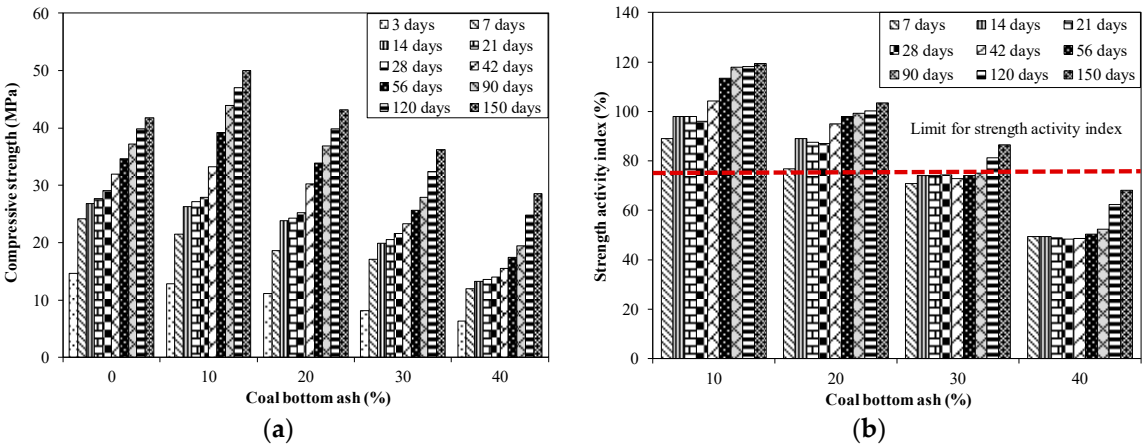

Figure 7. Compressive strength and strength activity index results for specimens incorporating various proportions of CBA. (**a**) Compressive strength, and (**b**) Strength activity index.

For mixtures incorporating higher CBA dosage (30% and 40% by cement mass), a decreasing trend in compressive strength was observed compared to that of the control specimens without CBA

at all testing ages. For example, 28 days $f'c$ was 21 and 14 MPa for mixtures incorporating 30% and 40% of CBA, respectively, compared to 29 MPa for the control specimens. This is likely due to OPC dilution [21,87,88], leading to limited hydration reactions and increased porosity (Figure 8) and decreased strength [23,101]. Abbas et al. [21] reported 55% decrease in 28 days $f'c$ for a mixture incorporating 40% sugarcane bagasse ash (SBA) compared to that of the control mixture without SBA. Additionally, Saha and Sarker [19] reported 39% decrease in 28 days $f'c$ for specimens incorporating 30% fly ash (FA) compared to that of control specimens without FA. Aydin [86] reported 29% decrease in 28 days $f'c$ due to incorporation of CBA. Such results indicate that high levels of OPC replacement limit the cement hydration and the CH available for pozzolanic reactions, leading to a decay in $f'c$.

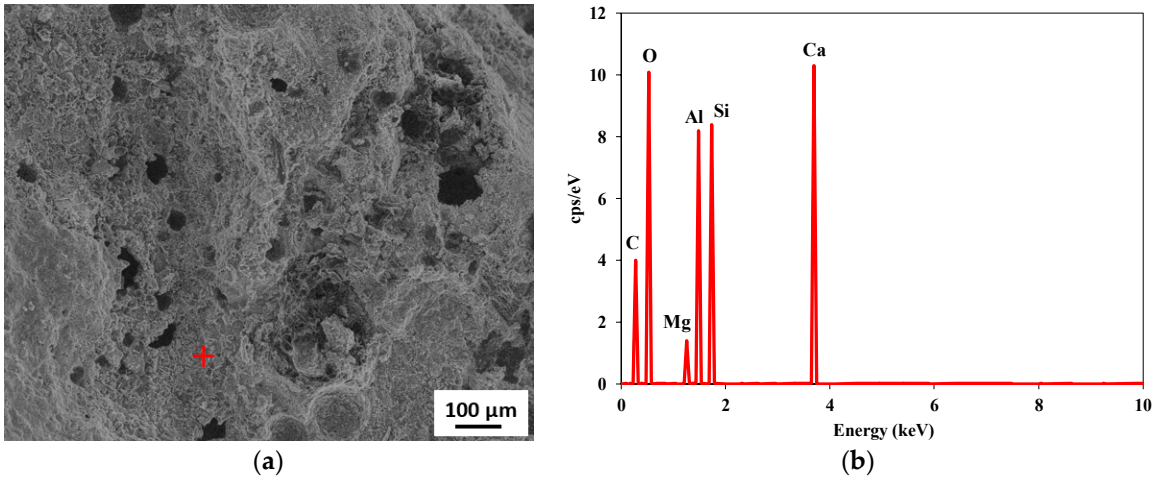

Figure 8. Scanning electron microscopy image of specimen incorporating 30% CBA. (**a**) Pores in specimen with 30% of CBA, and (**b**) EDX at (+).

Figure 7b shows the strength activity index (SAI) results for specimens incorporating various proportions of untreated CBA. For the mixture incorporating 10% CBA, SAI was 95% at 28 days, but increased to 120% at 150 days. SAI was around 86% at 28 days, then increased to 103% at 150 days for specimens incorporating 20% CBA. Specimens incorporating 40% CBA had SAI less than 75% at all testing ages (Figure 7b). According to ASTM C311 [54] and BS EN-450 [102], in mixtures with SAI > 75%, CBA can be considered pozzolanic. CBA up to 20% by cement weight can be effectively used without compromising mechanical strength. Similar results were found in previous studies. For example, Saha and Sarker [6] reported 84% SAI at 28 days for specimens incorporating 10% fly ash, which decreased to 61% for specimens incorporating 30% fly ash. Oruji et al. [67] reported 108% and 119% SAI at 28 and 90 days for mixtures made with 20% pulverized CBA.

Figure 9 shows flexural strength (f_r) results for mixtures incorporating various proportions of CBA. Reported f_r results are average values obtained on four identical specimens with COV < 3%. A continuous increase in f_r was observed with curing age. For example, f_r was 8.38, 10.05, 10.65, 11.50 and 12.68 MPa at 14, 28, 56, 90 and 150 days, respectively. Munir et al. [103] reported comparable 28 days f_r results. For specimens incorporating 10% CBA, f_r was 10.90 and 12.55 MPa at 90 and 150 days, respectively, which is comparable to results of control specimens without CBA. However, f_r decreased at all test ages for specimens incorporating higher proportions of CBA. For instance, 38% decrease in f_r was recorded for specimens incorporating 30% CBA compared to that of the control specimens, which can be attributed to cement dilution. Aydin [86] reported 27% decrease in 28 days f_r for specimens incorporating CBA. However, relatively less reduction in flexural strength due to incorporation of CBA was observed at later ages (i.e., 150 days). For example, f_r decreased by 5% for specimens incorporating 20% CBA at 150 days compared to 17% reduction at 28 days. Similar results were reported in previous study [28].

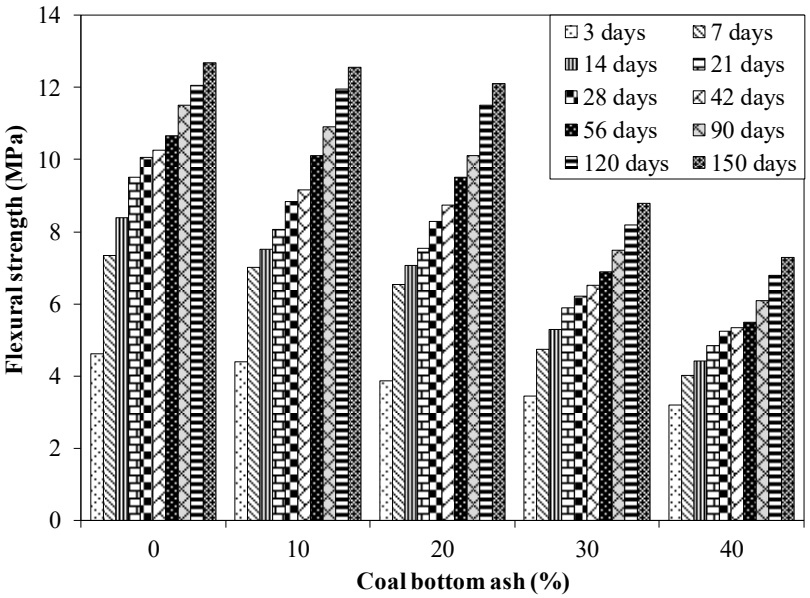

Figure 9. Flexural strength results for specimens incorporating various proportions of CBA.

3.6. Expansion Due to ASR

Figure 10 illustrates mortar bar expansion results for specimens incorporating various proportions of untreated CBA. Each result is the average value of five identical specimens, with COV <2.9%, which is within the limits of ASTM C1260 [41]. The mortar bar expansion at 14 and 28 days was 0.23% and 0.28% for control specimens without CBA, respectively. Thus, the aggregates can be classified as reactive according to ASTM C1260 [41] since the mortar bar expansion was greater than 0.10% and 0.20% at 14 and 28 days, respectively. Results show decreasing ASR expansion for mixtures incorporating CBA. For instance, specimens incorporating 10% CBA had expansion of 0.17% and 0.22% at 14 and 28 days, respectively, which is still higher than the allowable limit of ASTM C1260 (Figure 10b). Specimens incorporating 20% CBA incurred expansion of 0.19% at 28 days, which is less than the ASTM limit. Expansion at 28 days was 0.17% for specimens made with 40% CBA. This reduction in expansion can be attributed to the pozzolanic reaction of CBA leading to consumption of portlandite and formation of more negatively charged calcium silicate hydrates (CSH), which bind alkalis, leading to decreased alkalinity of the pore solution and less ASR expansion [17,19,103]. The high temperature of the test (80 °C) likely increased pozzolanic reaction, enhancing its effectiveness [59]. Several previous studies reported similar findings for SCMs mitigating ASR expansion. For instance, Abbas et al. [21] reported 30% decrease in ASR expansion for mixture incorporating 30% sugarcane bagasse ash compared to that of control specimens. Saha and Sarker [19] reported 34% reduction in ASR expansion at 64 days for mixture with 10% fly ash. Similarly, Esteves et al. [60] identified reduction in ASR expansion due to incorporation of CBA.

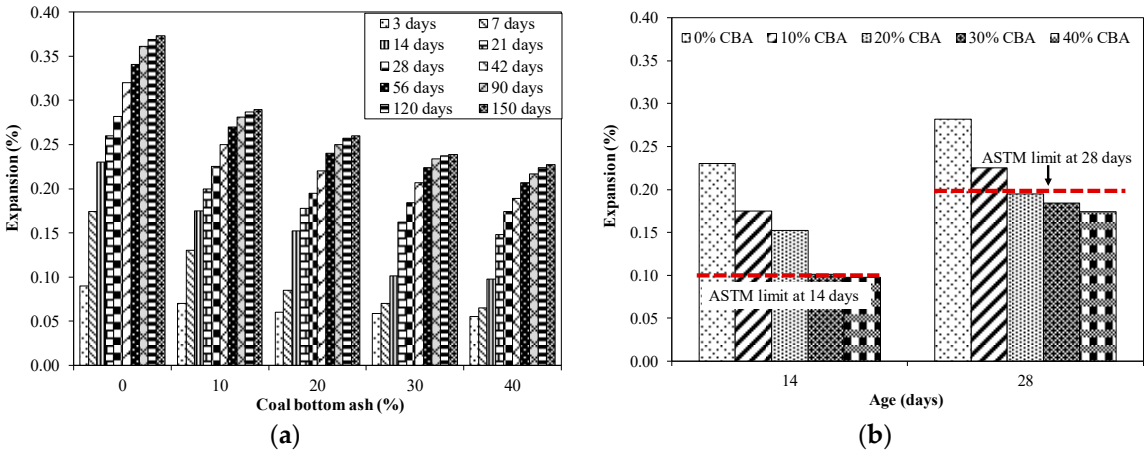

Figure 10. Expansion results and ASTM limits for mixture with various proportions of CBA. (**a**) Expansion results, and (**b**) ASTM limits for expansion.

It was observed that expansion increased with time for all tested mixtures (Figure 10). For instance, expansion was 0.37% for control specimens at 150 days compared to 0.28% at 28 days, as observed in previous studies [19,67,104,105]. Additionally, the rate of increase in expansion with time was less for specimens incorporating CBA (Figure 10). Mortar bar specimens were visually inspected to observe any surface distress due to ASR. The control specimens showed noticeable surface cracks at 150 days, indicating detrimental ASR expansion. Mortar bar specimens incorporating 20%, 30% and 40% CBA showed no sign of surface distress or cracking, which is consistent with expansion measurements.

According to the Australian Standard AS-1141.60.1 [106], if mortar bar expansion at 10 and 21 days is less than 0.10% and 0.30% respectively, ASR reaction could be considered low. Additionally, aggregates can be considered non-reactive if the mortar bar expansion is less than 0.10% at 28 days [106]. Moreover, if expansion is less than 0.10% at 16 days, specimens can be considered non-reactive in accordance with RILEM AAR-2 (2016) [107]. In the present study, control specimens had expansion greater than 0.10% at 10 days; therefore, can be considered as reactive according to Australian and RILEM standards. Mixture incorporating 20% CBA had expansion of less than 0.10% and 0.30% at 10 and 21 days, respectively. Therefore, it can be posited that CBA was efficient in mitigating ASR expansion with added benefit of limiting the environmental overburden landfilling CBA.

3.7. Effect of ASR on Compressive and Flexural Strengths

Figure 11 illustrates reduction in compressive and flexural strengths due to ASR exposure for specimens incorporating various proportions of CBA. Specimens exposed to ASR conducive conditions (NaOH solution at 80 °C) had lower $f'c$ compared to that of identical specimens placed in a normal curing regime. For example, control specimens without CBA incurred 16% decrease in $f'c$ at 150 days in the ASR conductive environment compared to that of similar specimens placed in curing water. This can be attributed to the formation of ASR gel and associated microcracks. Similar reduction in $f'c$ for specimens subjected to ASR conducive exposure were reported in previous studies [108,109]. However, specimens incorporating CBA placed in ASR conditions incurred less reduction in $f'c$. For instance, specimens made with 20% CBA subjected to ASR conditions had 10% decrease in $f'c$ at 150 days compared to identical specimens cured in water. Saha and Sarker [19] reported 12% reduction in $f'c$ for specimens incorporating 20% fly ash subjected to NaOH solution at 80 °C. It was predicted that ASR conducive exposure can reduce $f'c$ by 20% after one-year expansion of 0.28% [105]. Similarly, reduction in flexural strength was observed for specimens exposed to ASR conducive environment compared to that of specimens placed in normal water (Figure 11b). For example, approximately 14% decrease in flexural strength was observed at 150 days for control specimens exposed to ASR conditions compared to identical specimens placed in water. Generally, less reduction in flexural strength was observed for specimens incorporating CBA.

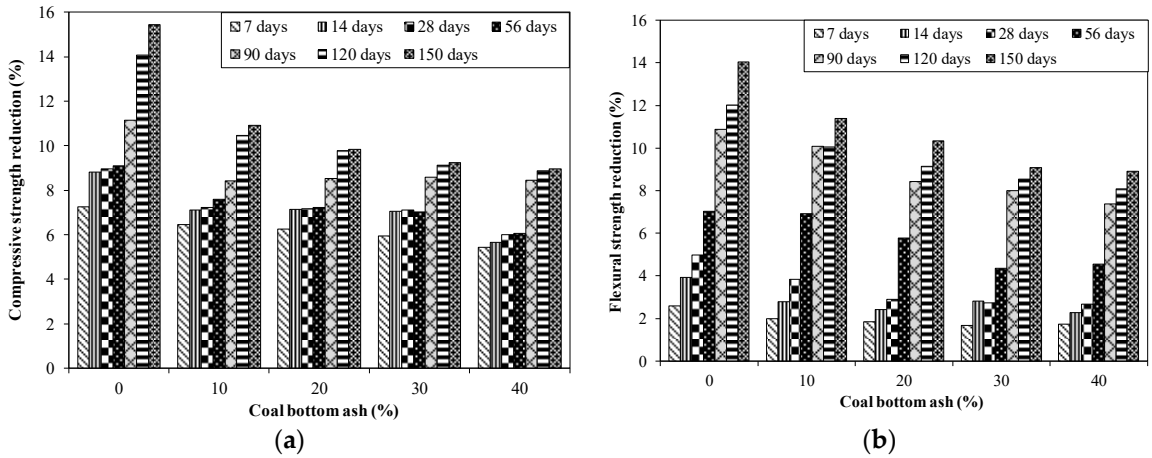

Figure 11. Effect of ASR conditions on compressive and flexural strengths of specimens incorporating various proportions of CBA. (**a**) Compressive strength, and (**b**) flexural strength.

3.8. Microstructural and EDX Analyses

Microstructural examination of specimens exposed to NaOH solution showed formation of ASR gel. ASR gel tends to absorb surrounding moisture and swell, inducing distress and microcracking. Micro-cracks were observed around aggregate interfaces (Figure 12).

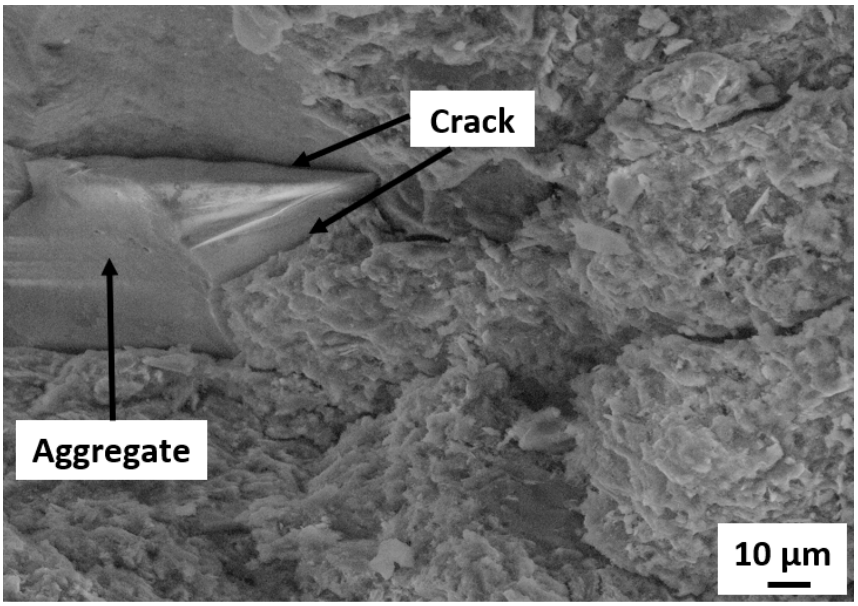

Figure 12. SEM image of cracks around aggregate in control specimen immersed in NaOH solution.

The formation of ASR products can alter microstructural and mechanical properties of concrete due to development of cracks, which may propagate towards the concrete surface, accelerating the penetration of hostile media such as chloride ions, thus compromising durability and structural integrity. Figure 13 shows SEM images and EDX analysis of control specimens after 56 days of immersion in NaOH solution. Microcracks can be observed in the control specimens, surrounded by ASR gel (rich in calcium, silica and alkalis) with various morphologies, as confirmed through EDX analysis.

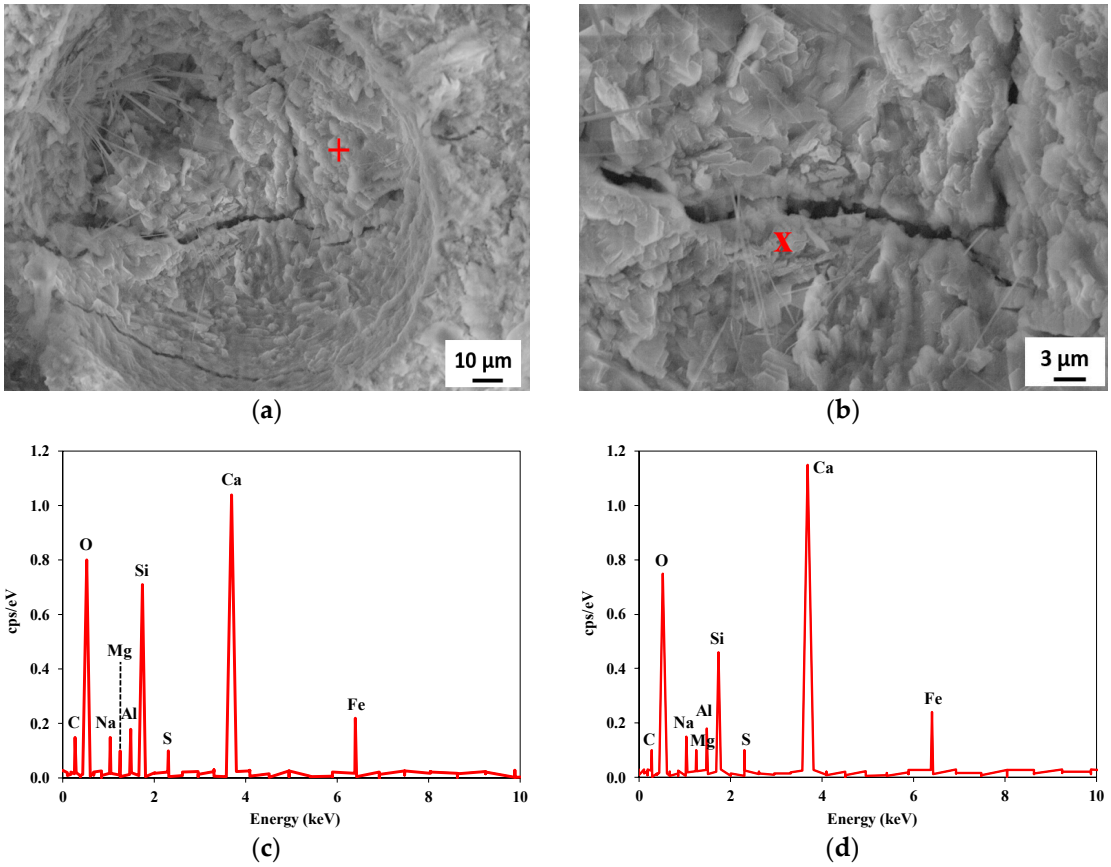

Figure 13. SEM and EDX analyses of control specimen without CBA at 56 days immersion in NaOH solution. (**a**,**b**) Cracking in control specimens subjected to ASR conditions, (**c**) EDX at (+), and (**d**) EDX at (x).

The observed ASR gel had calcium-to-silica ratio (Ca/Si), sodium-to-silica ratio (Na/Si) and aluminum-to-silica ratio (Al/Si) of 3.20, 0.30 and 0.035, respectively, similar to previous studies [110,111]. ASR products appeared in the form of a network having fibrous morphology (Figure 14). EDX analysis showed that it was constituted of calcium, silica and alkalis. ASR gel filled micropores in specimens incorporating porous CBA, which showed denser structure after 56 days of immersion in the NaOH solution compared to that of control specimens without CBA.

The interfacial region between aggregates and cementitious matrix was dense and compact for specimens incorporating 20% of CBA exposed to 56 days of NaOH solution (Figure 15), with no observed cracks or voids, as in previous study [104]. Amorphous silica in CBA likely reacted earlier with the alkalis present in the pore solution, mitigating the reaction between aggregates, and thus limiting the formation of ASR gel [104]. Specimens incorporating 40% CBA showed little sign of ASR products, indicating the efficiency of CBA. Beglarigale and Yazici [112] reported that specimens incorporating 40% of GGBS had no indication of ASR gel. Similarly, Saha and Sarker [19] reported no cracking due to ASR exposure in specimens made with fly ash.

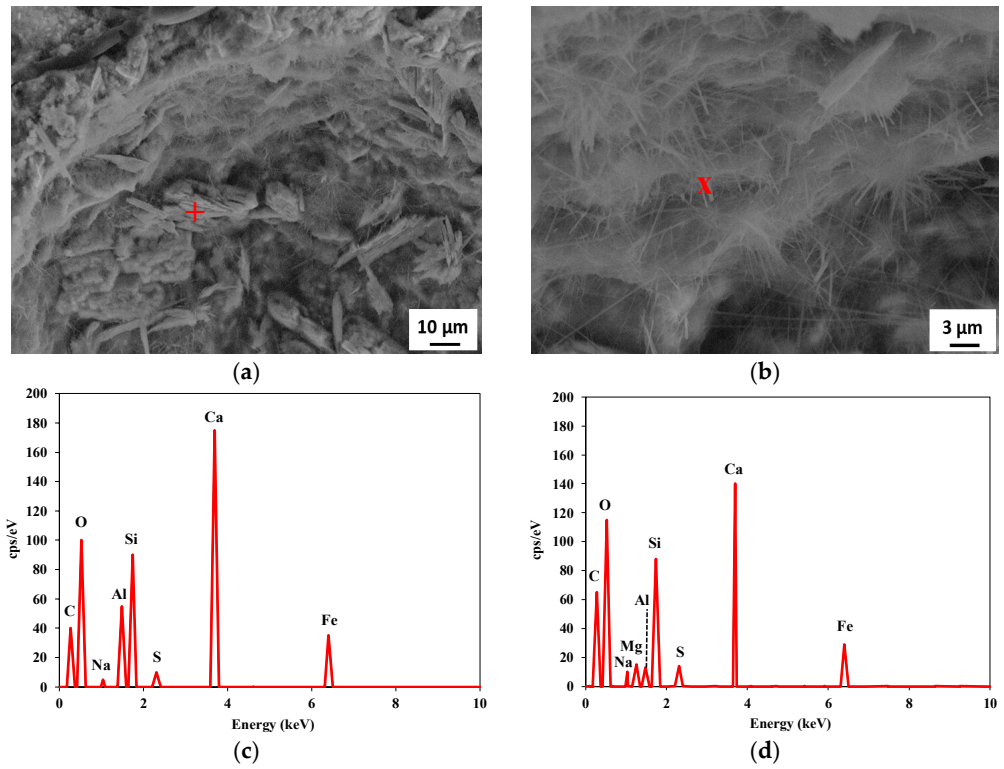

Figure 14. SEM image and EDX of ASR gel. (**a**,**b**) ASR network, (**c**) EDX at (+), and (**d**) EDX at (x).

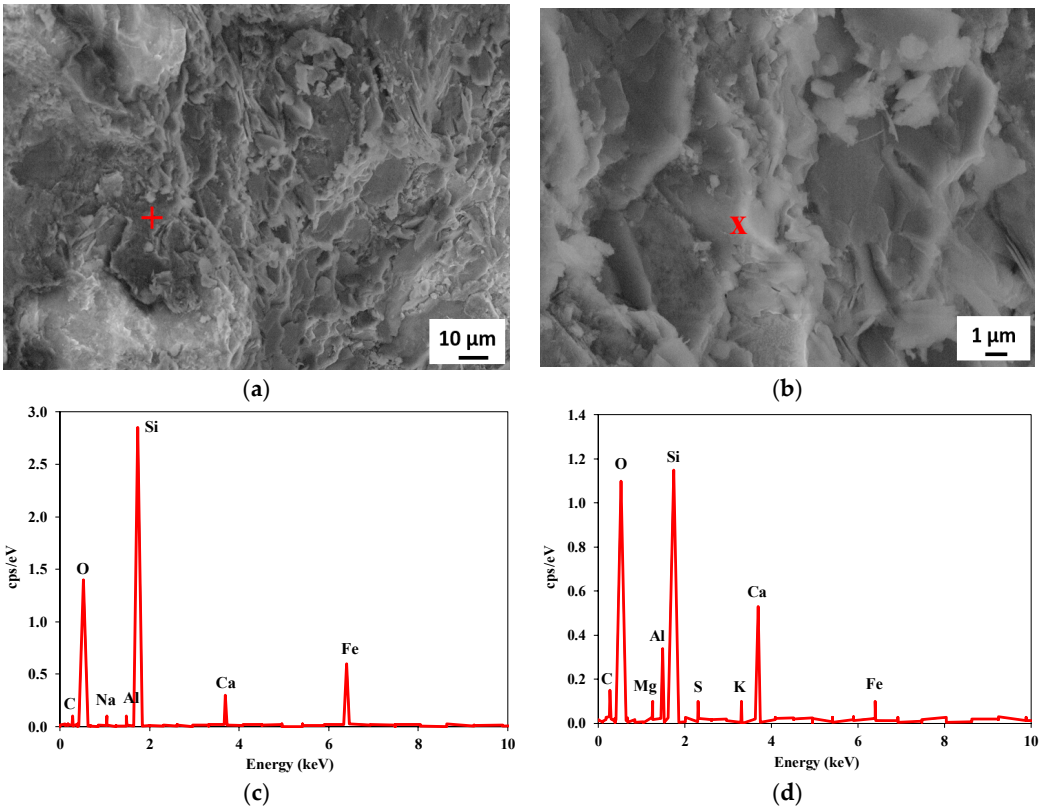

Figure 15. SEM images and EDX of specimen incorporating 20% of CBA subjected to ASR condition. (**a**,**b**) SEM images of specimen incorporating 20% of CBA, (**c**) EDX at (+), and (**d**) EDX at (x).

4. Conclusions

This study explored the pozzolanic behavior of local untreated coal bottom ash (CBA) and its role in controlling alkali–silica reaction (ASR) expansion. Specimens incorporating various proportions of untreated CBA (0% to 40% by cement mass) were investigated for up to 150 days. The used CBA was porous with high LOI (>10%). CBA had heavy metals content of less than standard limits. Thus, it can be considered non-hazardous. The used aggregates were ASR reactive, as confirmed by petrographic analysis. Based on the experimental results, the following conclusions can be drawn:

- The flow of mortar mixtures incorporating CBA decreased compared to that of the control mixture without CBA, likely due to the porous nature of CBA and its high unburnt content.
- The 28 days $f'c$ of specimens incorporating 10% CBA was comparable to that of the control specimens without CBA. At later ages (>28 days), an increase in compressive strength for specimens incorporating 10% CBA was observed compared to that of the control specimens. Higher CBA proportions (i.e., 30% and 40%) led to decreased $f'c$ at all testing ages due to cement dilution.
- Specimens incorporating 10% and 20% CBA had strength activity index (SAI) greater than 75%, confirming the pozzolanic nature of CBA.
- Mortar bar specimens without CBA had 0.23% and 0.28% of ASR expansion at 14 and 28 days, respectively, higher than the limits specified by ASTM C1260. The maximum expansion was 0.37% for the control specimens without CBA at 150 d.
- Specimens incorporating CBA exhibited less ASR expansion compared to that of the control specimens. For instance, mortar bars incorporating 40% CBA had expansion of 0.09% and 0.17% at 14 and 28 days, respectively.
- SEM images showed ASR microcracks in control specimens without CBA. However, specimens incorporating CBA showed no microcracking and denser microstructure.
- Using CBA as partial replacement for cement can decrease the energy consumed in cement manufacturing and the associated CO_2 emissions, reduce the landfilling of CBA, while mitigating ASR expansion and the associated costly damage in concrete structures.

In short, it can be concluded that the locally produced untreated CBA can be effectively utilized in controlling the ASR expansion. Moreover, incorporating a low dosage of local CBA (i.e., 10% by cement mass) had insignificant effect on the compressive and flexural strengths. However, high CBA proportions (i.e., 30% and 40%) decreased the compressive and flexural strengths at all testing ages. Under ASR controlled conditions, the compressive and flexural strengths of specimens were less than that of identical specimens placed in normal curing. However, this strength loss was less significant for specimens incorporating untreated CBA. This study serves as a benchmark for investigating locally produced CBA from thermal power plants for sustainable construction applications. It is believed that the beneficiation of CBA and grinding it to finer particle size can achieve better results than those reported in the present study. However, this needs future dedicated study.

Author Contributions: Conceptualization, S.A. and M.L.N.; methodology, S.A. and M.L.N.; validation, S.A. and M.L.N.; formal analysis, U.A., W.A., A.A. and S.A.; investigation, U.A., W.A., A.A. and S.A.; resources, S.A.; data curation, U.A., W.A. and A.A.; writing—original draft preparation, U.A., W.A., A.A. and S.A.; writing—review and editing, M.L.N. and S.A.; visualization, U.A., W.A., A.A. and S.A.; supervision, S.A. and M.L.N.; project administration, S.A.; funding acquisition, S.A. and A.A. All authors have read and agreed to the published version of the manuscript.

Funding: This research was funded by the Higher Education Commission (HEC) of Pakistan through the National Research Program for Universities (NRPU) 9820 grant "Mitigation of Alkali-Silica Reaction Using Waste Materials: A Sustainable Approach".

Acknowledgments: The authors would like to acknowledge the support of the Department of Civil Engineering of the University of Engineering and Technology, Lahore.

Conflicts of Interest: The authors declare no conflict of interest.

References

1. ACI Committee 221. State-of-the-art report on alkali-aggregate reactivity. *Am. Concr. Inst.* **1998**, *221*, 1–23.
2. Giebson, C.; Voland, K.; Meng, B.; Ludwig, H.-M. Alkali-silica reaction performance testing of concrete considering external alkalis and preexisting microcracks. *Struct. Concr.* **2017**, *18*, 528–538. [CrossRef]
3. Wiedmann, A.; Weise, F.; Kotan, E.; Müller, H.S.; Meng, B. Effects of fatigue loading and alkali-silica reaction on the mechanical behavior of pavement concrete. *Struct. Concr.* **2017**, *18*, 539–549. [CrossRef]
4. Chatterji, S. The role of $Ca(OH)_2$ in the breakdown of Portland cement concrete due to alkali-silica reaction. *Cem. Concr. Res.* **1979**, *9*, 185–188. [CrossRef]
5. Na, O.; Xi, Y.; Ou, E.; Saouma, V.E. The effects of alkali-silica reaction on the mechanical properties of concretes with three different types of reactive aggregate. *Struct. Concr.* **2016**, *17*, 74–83. [CrossRef]
6. Saha, A.K.; Sarker, P.K. Expansion due to alkali-silica reaction of ferronickel slag fine aggregate in OPC and blended cement mortars. *Constr. Build. Mater.* **2016**, *123*, 135–142. [CrossRef]
7. Ono, K. Damaged concrete structures in Japan due to alkali silica reaction. *Int. J. Cem. Compos. Light. Concr.* **1988**, *10*, 247–257. [CrossRef]
8. Stark, D. *Handbook for the Identification of Alkali-Silica Reactivity in Highway Structures*; SHRP-C/FR-91-101; TRB National Research Council: Washington, DC, USA, 1991; p. 49.
9. Thomas, M.; Folliard, K.J.; Fournier, B.; Rivard, P.; Drimalas, T. *Methods for Evaluating and Treating ASR-Affected Structures: Results of Field Application and Demonstration Projects, 2013b Volume II: Details of Field Applications and Analysis (Report FHWA-HIF-14-003)*; Federal Highway Administration (FHWA), U.S. Dept of Transportation: Washington, DC, USA, 2013; p. 342.
10. Owsiak, Z.; Zapała-Sławeta, J.; Czapik, P. Diagnosis of concrete structures distress due to alkali-aggregate reaction. *Bull. Pol. Acad. Sci. Technic. Sci.* **2015**, *63*, 23–29. [CrossRef]
11. Jensen, V. Alkali–silica reaction damage to Elgeseter Bridge, Trondheim, Norway: A review of construction, research and repair up to 2003. *Mater. Charact.* **2004**, *53*, 155–170. [CrossRef]
12. Munir, M.J.; Qazi, A.U.; Kazmi, S.M.S.; Khitab, A.; Ashiq, S.Z.; Ahmed, I. A literature review on alkali silica reactivity of concrete in Pakistan. *Pak. J. Sci.* **2016**, *68*, 53–62.
13. Gocevski, V.; Pietruszczak, S. Assessment of the effects of slot cutting in concrete dams affected by alkali aggregate reaction. In Proceedings of the 11th International Conference on Alkali Aggregate Reaction in Concrete, Quebec City, QC, Canada, 11–16 June 2000; pp. 1303–1312.
14. Cavalcanti, A.; Campos, A.; Silveria, E.; Wanderley, E. Rehabilitation of a generating unit affected by alkali-aggregate reaction. In Proceedings of the 11th International Conference on Alkali-Aggregate Reaction in Concrete, Quebec City, QC, Canada, 11–16 June 2000; pp. 1253–1262.
15. US. Geological Survey. *Mineral Commodity Summaries 2015. USA Geological. Survey*; US. Geological Survey: Reston, VI, USA, 2015.
16. Choate, W.T. Energy and Emission Reduction Opportunities for the Cement Industry. In *Energy and Emission Reduction Opportunities for the Cement Industry*; Office of Scientific and Technical Information (OSTI): Washington, DC, USA, 2003.
17. Thomas, M. The effect of supplementary cementing materials on alkali-silica reaction: A review. *Cem. Concr. Res.* **2011**, *41*, 1224–1231. [CrossRef]
18. Shehata, M.H.; Thomas, M.D.; Bleszynski, R.F. The effects of fly ash composition on the chemistry of pore solution in hydrated cement pastes. *Cem. Concr. Res.* **1999**, *29*, 1915–1920. [CrossRef]
19. Saha, A.K.; Sarker, P.K.; Potential, A.S.R. expansion mitigation of ferronickel slag aggregate by fly ash. *Struct. Concr.* **2018**, *19*, 1376–1386. [CrossRef]
20. Abbas, S.; Kazmi, S.M.; Munir, M.J. Potential of rice husk ash for mitigating the alkali-silica reaction in mortar bars incorporating reactive aggregates. *Constr. Build. Mater.* **2017**, *132*, 61–70. [CrossRef]
21. Abbas, S.; Sharif, A.; Ahmed, A.; Abbass, W.; Shaukat, S. Prospective of sugarcane bagasse ash for controlling ASR in concrete incorporating reactive aggregates. *Structut. Concr.* **2019**, *1*, 1–13.
22. Rafieizonooz, M.; Mirza, J.; Salim, M.R.; Hussin, M.W.; Khankhaje, E. Investigation of coal bottom ash and fly ash in concrete as replacement for sand and cement. *Constr. Build. Mater.* **2016**, *116*, 15–24. [CrossRef]
23. Hashemi, S.S.G.; Bin Mahmud, H.; Djobo, J.N.Y.; Tan, C.G.; Ang, B.C.; Ranjbar, N. Microstructural characterization and mechanical properties of bottom ash mortar. *J. Clean. Prod.* **2018**, *170*, 797–804. [CrossRef]

24. Singh, N.; Shehnaz, D.; Bhardwaj, A. Reviewing the role of coal bottom ash as an alternative of cement. *Constr. Build. Mater.* **2020**, *233*, 117276. [CrossRef]
25. Izquierdo, M.; Querol, X. Leaching behaviour of elements from coal combustion fly ash: An overview. *Int. J. Coal Geol.* **2012**, *94*, 54–66. [CrossRef]
26. Sushil, S.; Batra, V. Analysis of fly ash heavy metal content and disposal in three thermal power plants in India. *Fuel* **2006**, *85*, 2676–2679. [CrossRef]
27. Abdulmatin, A.; Tangchirapat, W.; Jaturapitakkul, C. An investigation of bottom ash as a pozzolanic material. *Constr. Build. Mater.* **2018**, *186*, 155–162. [CrossRef]
28. Kurama, H.; Kaya, M. Usage of coal combustion bottom ash in concrete mixture. *Constr. Build. Mater.* **2008**, *22*, 1922–1928. [CrossRef]
29. American Coal bottom ash Association; 99/03527 Current trends in coal combustion product (CCP) production and use. *Fuel Energy Abstr.* **1999**, *40*, 376. [CrossRef]
30. Kou, S.-C.; Poon, C.-S. Properties of concrete prepared with crushed fine stone, furnace bottom ash and fine recycled aggregate as fine aggregates. *Constr. Build. Mater.* **2009**, *23*, 2877–2886. [CrossRef]
31. Qiao, X.; Tyrer, M.; Poon, C.; Cheeseman, C. Novel cementitious materials produced from incinerator bottom ash. *Resour. Conserv. Recycl.* **2008**, *52*, 496–510. [CrossRef]
32. Zhang, B.; Poon, C.S. Use of Furnace Bottom Ash for producing lightweight aggregate concrete with thermal insulation properties. *J. Clean. Prod.* **2015**, *99*, 94–100. [CrossRef]
33. Kim, H.; Lee, H. Use of power plant bottom ash as fine and coarse aggregates in high-strength concrete. *Constr. Build. Mater.* **2011**, *25*, 1115–1122. [CrossRef]
34. Oruji, S.; Brake, N.A.; Guduru, R.K.; Nalluri, L.; Günaydın-Şen, Ö.; Kharel, K.; Rabbanifar, S.; Hosseini, S.; Ingram, E. Mitigation of ASR expansion in concrete using ultra-fine coal bottom ash. *Constr. Build. Mater.* **2019**, *202*, 814–824. [CrossRef]
35. Gooi, S.; Mousa, A.; Kong, D. A critical review and gap analysis on the use of coal bottom ash as a substitute constituent in concrete. *J. Clean. Prod.* **2020**, *268*, 121752. [CrossRef]
36. Muthusamy, K.; Jamaludin, N.F.A.; Kamaruzzaman, M.N.; Ahmad, M.Z.; Zamri, N.A.; Budiea, A.M.A. *Compressive Strength of Palm Oil Clinker Lightweight Aggregate Concrete Containing Coal bottom Ash as Sand Replacement*; Elsevier BV: Amsterdam, The Netherlands, 2020.
37. Arun, N.; Singh, P.; Gupta, S. Utilization of ground bottom ash in concrete. *Mater. Today Proc.* **2020**, *32*, 663–669. [CrossRef]
38. Yao, Z.; Ji, X.; Sarker, P.; Tang, J.H.; Ge, L.; Xia, M.; Xi, Y. A comprehensive review on the applications of coal fly ash. *Earth Sci. Rev.* **2015**, *141*, 105–121. [CrossRef]
39. *Private Power and Infrastructure Board, Pakistan Coal Power Generation Potential*; Government of Pakistan: Islamabad, Pakistan, 2004; p. 77.
40. Coutinho, M.; Butt, H.K. *Environmental Impact Assessment Guidance for Coal Fired Power Plants in Pakistan*; IUCN: Islamabad, Pakistan, 2014; p. 149.
41. ASTM C1260. *Standard Test Method for Potential Alkali Reactivity of Aggregates (Mortar-Bar Method)*; American Society for Testing and Materials: West Conshohocken, PA, USA, 2014; p. 5.
42. ASTM C184. *Standard Test Method for Fineness of Hydraulic Cement by the 150 Micrometer (no. 100) and 75 Micrometer (no. 200) Sieves*; ASTM: West Conshohocken, PA, USA, 1994; p. 3.
43. ASTM C204. *Standard Test Methods for Fineness of Hydraulic Cement by Air Permeability Apparatus*; American Society for Testing and Materials: West Conshohocken, PA, USA, 2018; p. 11.
44. ASTM C188. *Standard Test Method for Density of Hydraulic Cement*; American Society for Testing and Materials: West Conshohocken, PA, USA, 2017; p. 3.
45. ASTM C151. *Standard Test Method for Autoclave Expansion of Hydraulic Cement*; American Society for Testing and Materials: West Conshohocken, PA, USA, 2018; p. 4.
46. ASTM C295. *Standard Guide for Petrographic Examination of Aggregates for Concrete*; American Society for Testing and Materials: West Conshohocken, PA, USA, 2019; p. 9.
47. USEPA. TCLP Method 1311. *Eff. Br. Mind. Interv. Acute Pain Exp. AnExam. Individ. Differ.* **2015**, *1*, 1–36.
48. Rafieizonooz, M.; Salim, M.R.; Mirza, J.; Hussin, M.W.; Salmiati, R.; Khan, E.K. Toxicity characteristics and durability of concrete containing coal bottom ash assubstitute for cement and river sand. *Construct. Build. Mater.* **2017**, *143*, 234–246. [CrossRef]

49. ASTM C187. *Standard Test Method for Amount of Water Required for Normal Consistency of Hydraulic Cement Paste*; American Society for Testing and Materials: West Conshohocken, PA, USA, 2016; p. 3.
50. ASTM C191. *Standard Test Methods for Time of Setting of Hydraulic cement by Vicatneedle*; American Society for Testing and Materials: West Conshohocken, PA, USA, 2019; p. 8.
51. ASTM C1437. *Standard Test Method for Flow of Hydraulic Cement Mortar*; American Society for Testing and Materials: West Conshohocken, PA, USA, 2015; p. 2.
52. ASTM C109. *Standard Test Method for Compressive Strength of Hydraulic Cement Mortars (Using 2in. or [50 mm] Cube Specimens)*; ASTM: West Conshohocken, PA, USA, 2016; p. 10.
53. ASTM C348. *Standard Test Method for Flexural Strength of Hydraulic Cement Mortars*; American Society for Testing and Materials: West Conshohocken, PA, USA, 2019; p. 6.
54. ASTM C311. *Standard Test Methods for Sampling and Testing Fly Ash or Natural Pozzolans for Use in Portland Cement Concrete*; ASTM: West Conshohocken, PA, USA, 2018; p. 11.
55. ASTM C642. *Standard Test Method for Density, Absorption, and Voids in Hardened Concrete*; ASTM: West Conshohocken, PA, USA, 2013; p. 3.
56. ASTM C490. *Standard Practice for Use of Apparatus for the Determination of Length Change of Hardened Cement Paste, Mortar, and Concrete*; ASTM: West Conshohocken, PA, USA, 2017; p. 5.
57. Jaturapitakkul, C.; Cheerarot, R. Development of Bottom Ash as Pozzolanic Material. *J. Mater. Civ. Eng.* **2003**, *15*, 48–53. [CrossRef]
58. Muthusamy, K.; Rasid, M.H.; Jokhio, G.A.; Budiea, A.M.A.; Hussin, M.W.; Mirza, J. Coal bottom ash as sand replacement in concrete: A review. *Constr. Build. Mater.* **2020**, *236*, 117507. [CrossRef]
59. Wu, Z.; Naik, T. *Use of Clean Coal bottom Ash for Managing ASR. Report No. CBU-2004-06, 2004*; Civil Engineering Department, The University of Wisconsin-Milwaukee: Milwaukee, WI, USA, 2004; p. 12.
60. Esteves, T.; Rajamma, R.; Soares, D.; Silva, A.S.; Ferreira, V.; Labrincha, J.A. Use of biomass fly ash for mitigation of alkali-silica reaction of cement mortars. *Constr. Build. Mater.* **2012**, *26*, 687–693. [CrossRef]
61. Kim, H.-K. Utilization of sieved and ground coal bottom ash powders as a coarse binder in high-strength mortar to improve workability. *Constr. Build. Mater.* **2015**, *91*, 57–64. [CrossRef]
62. Targan, Ş.; Olgun, A.; Erdogan, Y.; Sevinc, V. Effects of supplementary cementing materials on the properties of cement and concrete. *Cem. Concr. Res.* **2002**, *32*, 1551–1558. [CrossRef]
63. Targan, S.; Olgun, A.; Erdogan, Y.; Sevinç, V. Influence of natural pozzolan, colemanite ore waste, bottom ash, and fly ash on the properties of Portland cement. *Cem. Concr. Res.* **2003**, *33*, 1175–1182. [CrossRef]
64. Chusilp, N.; Jaturapitakkul, C.; Kiattikomol, K. Effects of LOI of ground bagasse ash on the compressive strength and sulfate resistance of mortars. *Constr. Build. Mater.* **2009**, *23*, 3523–3531. [CrossRef]
65. Siddique, R. Compressive strength, water absorption, sorptivity, abrasion resistance and permeability of self-compacting concrete containing coal bottom ash. *Constr. Build. Mater.* **2013**, *47*, 1444–1450. [CrossRef]
66. Singh, M.; Siddique, R. Strength properties and micro-structural properties of concrete containing coal bottom ash as partial replacement of fine aggregate. *Constr. Build. Mater.* **2014**, *50*, 246–256. [CrossRef]
67. Oruji, S.; Brake, N.A.; Nalluri, L.; Guduru, R.K. Strength activity and microstructure of blended ultra-fine coal bottom ash-cement mortar. *Constr. Build. Mater.* **2017**, *153*, 317–326. [CrossRef]
68. Cheriaf, M.; Rocha, J.; Péra, J. Pozzolanic properties of pulverized coal combustion bottom ash. *Cem. Concr. Res.* **1999**, *29*, 1387–1391. [CrossRef]
69. Andrade, L.; Rocha, J.; Cheriaf, M. Influence of coal bottom ash as fine aggregate on fresh properties of concrete. *Constr. Build. Mater.* **2009**, *23*, 609–614. [CrossRef]
70. USEPA (United States Environmental Protection Agency). *US Environmental Protection Agency Method 1311*; USAEPA: Washington, DC, USA, 1992.
71. USEPA. *Land Application of Sewage Sludge: A Guide for Land Appliers on the Requirements of the Federal Standards for the Use or Disposal of Sewage Sludge, 40 CFR Part 503" EPA/831-B-93-002b*; USEPA: Washington, DC, USA, 1994; p. 105.
72. U.S. Composting Council. *Test Methods for the Examination of Composting and Compost (Interim Draft)*; U.S. Composting Council: Bethesda, MD, USA, 1997.
73. Liu, A.; Ren, F.; Lin, W.Y.; Wang, J.-Y. A review of municipal solid waste environmental standards with a focus on incinerator residues. *Int. J. Sustain. Built Environ.* **2015**, *4*, 165–188. [CrossRef]

74. EUR-Lex, Council decision 2003/33/EC of December 2002. *Establishing Criteria and Procedures for the Acceptance of Waste at Landfills Pursuant to Article 16 of and Annex II to Director 1999/31/EC*; European Union: Brussels, Belgium, 20 December 2003.
75. Fytianos, K.; Tsaniklidi, B.; Voudrias, E. Leachability of heavy metals in Greek fly ash from coal combustion. *Environ. Int.* **1998**, *24*, 477–486. [CrossRef]
76. Wadge, A.; Hutton, M.; Peterson, P. The concentrations and particle size relationships of selected trace elements in fly ashes from U.K. coal-fired power plants and a refuse incinerator. *Sci. Total. Environ.* **1986**, *54*, 13–27. [CrossRef]
77. Hassaan, M.; El-Nemr, A.; Madkour, F. Environmental assessment of heavy metal pollution and human health risk. *Am. J. Water Sci. Eng.* **2016**, *2*, 14–19.
78. Sijakova-Ivanova, T.; Panov, Z.; Blazev, K.; Zajkova-paneva, V. Investigation of fly ash heavy metals content and physico chemical properties from thermal power plant, Republic of Macedonia. *Int. J. Eng. Sci. Technol. (IJEST)* **2011**, *3*, 8219–8225.
79. Llorens, J.F.; Fernandez-Turiel, J.; Querol, X. The fate of trace elements in a large coal-fired power plant. *Environ. Earth Sci.* **2001**, *40*, 409–416. [CrossRef]
80. Kumar, V.; Kumar, A.; Mathur, M. Management of fly ash in India: A perspective. In Proceedings of the third International Conference on Fly Ash Utilization and Disposal, New Dehli, India, 19–21 February 2003; pp. 1–18.
81. Gwenzi, W.; Mupatsi, N. Evaluation of heavy metal leaching from coal bottom ash versus conventional concrete monoliths and debris. *Waste Manag.* **2016**, *49*, 114–123. [CrossRef] [PubMed]
82. Danielowska, D. Heavy metals in fly ash from coal fired power station in Poland. *Pol. J. Environ. Studies* **2006**, *15*, 943–946.
83. Tharaniyil, R. *Coal Combustion Product Utilization Handbook*, 3rd ed.; WE Energies Publication: Amery, WI, USA, 2013; p. 448.
84. Dahl, O.; Poykio, R.; Nurmesniemi, H. Concentrations of heavy metals in fly ash from a coal-fired power plant with respect to the new Finnish limit values. *J. Mater. Cycles Waste Manag.* **2008**, *10*, 87–92. [CrossRef]
85. Singh, M.; Siddique, R. Effect of coal bottom ash as partial replacement of sand on properties of concrete. *Resour. Conserv. Recycl.* **2013**, *72*, 20–32. [CrossRef]
86. Aydin, E. Novel coal bottom ash waste composites for sustainable construction. *Constr. Build. Mater.* **2016**, *124*, 582–588. [CrossRef]
87. Mangi, S.; Ibrahim, M.; Jamaluddin, N.; Arshad, M.; Mudjanarko, S. Recycling of coal bottom ash in concrete as a partial cementitious resource. *Resources* **2019**, *8*, 1–10. [CrossRef]
88. Baite, E.; Messan, A.; Hannawi, K.; Tsobnang, F.; Prince, W. Physical and transfer properties of mortar containing coal bottom ash aggregates from Tefereyre (Niger). *Constr. Build. Mater.* **2016**, *125*, 919–926. [CrossRef]
89. Filho, C.G.D.S.; Milioli, F.E. A thermogravimetric analysis of the combustion of a Brazilian mineral coal. *Química Nova* **2008**, *31*, 98–103. [CrossRef]
90. Mal'chik, A.G.; Litovkin, S.V.; Rodionov, P.V. Investigations of physiochemical properties of bottom ash materials for use them as secondary raw materials. *Mater. Sci. Eng.* **2015**, *91*, 1–7.
91. Marinkovic, S.; Trifunovic, P.; Tobalic, R.; Matijasvic, S.; Kostic-Pulek, A. DTA/TGA studies of bottom ash from the Nikola Tesla power plant from Serbia for the purpose of its utilization in road construction. In Proceedings of the 36th International Conference of SSCHE, Matliare, Slovakia, 25–29 May 2009.
92. Dos Santos, R.P.; Martins, J.; Gadelha, C.; Cavada, B.; Albertini, A.V.; Arruda, F.; Vasconcelos, M.; Teixeira, E.; Alves, F.; Filho, J.L.; et al. Coal Fly Ash Ceramics: Preparation, Characterization, and Use in the Hydrolysis of Sucrose. *Sci. World J.* **2014**, *2014*, 1–7. [CrossRef] [PubMed]
93. Moropoulou, A.; Bakolas, A.; Aggelakopoulou, E. Evaluation of pozzolanic activity of natural and artificial pozzolans by thermal analysis. *Thermochim. Acta* **2004**, *420*, 135–140. [CrossRef]
94. Almeida, A.E.F.D.S.; Sichieri, E.P. Thermogravimetric analyses and mineralogical study of polymer modified mortar with silica fume. *Mater. Res.* **2006**, *9*, 321–326. [CrossRef]
95. Alarcon-Ruiz, L.; Platret, G.; Massieu, E.; Ehrlacher, A. The use of thermal analysis in assessing the effect of temperature on a cement paste. *Cem. Concr. Res.* **2005**, *35*, 609–613. [CrossRef]

96. Rajabipour, F.; Giannini, E.; Dunant, C.F.; Ideker, J.H.; Thomas, M.D. Alkali–silica reaction: Current understanding of the reaction mechanisms and the knowledge gaps. *Cem. Concr. Res.* **2015**, *76*, 130–146. [CrossRef]
97. Thomas, M. The role of calcium in alkali-silica reaction. In *Material Science of Concrete—The Sidney Diamond Symposium*; American Ceramic Society Bulletin: Westerville, OH, USA, 1998; pp. 325–337.
98. El-Jazairi, B.; Illston, J. A simultaneous semi-isothermal method of thermogravimetry and derivative thermogravimetry, and its application to cement pastes. *Cem. Concr. Res.* **1977**, *7*, 247–257. [CrossRef]
99. Aly, M.; Hashmi, M.; Olabi, A.; Messeiry, M.; Abadir, E.; Hussain, A. Effect of colloidal nano-silica on the mechanical and physical behaviour of waste-glass cement mortar. *Mater. Des.* **2012**, *33*, 127–135. [CrossRef]
100. Moser, R.D.; Jayapalan, A.R.; Garas, V.Y.; Kurtis, K.E. Assessment of binary and ternary blends of metakaolin and Class C fly ash for alkali-silica reaction mitigation in concrete. *Cem. Concr. Res.* **2010**, *40*, 1664–1672. [CrossRef]
101. Ranjbar, N.; Kuenzel, C. Influence of preheating of fly ash precursors to produce geopolymers. *J. Am. Ceram. Soc.* **2017**, *100*, 3165–3174. [CrossRef]
102. BS EN 450-1:2012. *Fly Ash for Concrete. Definition, Specifications and Conformity Criteria*; BSI: London, UK; p. 34.
103. Muhammad, J.; Munir, S.; Abbas, A.U.; Qazi, M.; Nehdi, S.M.; Kazmi, S. Role of test method in detection of aggregate ASR reactivity. *Inst. Civil Eng. (ICE) Construct. Mater. J.* **2016**, 1–19.
104. Saha, A.K. A comparative study between ASTM C1567 and ASTM C227 to mitigate alkali-silica reaction. *Struct. Concr.* **2019**, *20*, 420–427. [CrossRef]
105. Nagrockiene, D.; Rutkauskas, A. The effect of fly ash additive on the resistance of concrete to alkali silica reaction. *Constr. Build. Mater.* **2019**, *201*, 599–609. [CrossRef]
106. Wang, S. Cofired biomass fly ashes in mortar: Reduction of Alkali Silica Reaction (ASR) expansion, pore solution chemistry and the effects on compressive strength. *Constr. Build. Mater.* **2015**, *82*, 123–132. [CrossRef]
107. Australian Standard (AS) 1141.60.1. *Method for Sampling and Testing Aggregates, Potential Alkali-Silica Reactivity-Accelerated Mortar Bar Method*; Standards Australia: Sydney, Australia, 2014.
108. Nixon, P.J.; Sims, I. RILEM Recommended Test Method: AAR-2—Detection of Potential Alkali-Reactivity—Accelerated Mortar-Bar Test Method for Aggregates. *Alkali Activ. Mater.* **2015**, 61–77. [CrossRef]
109. Yazıcı, H. The effect of steel micro-fibers on ASR expansion and mechanical properties of mortars. *Constr. Build. Mater.* **2012**, *30*, 607–615. [CrossRef]
110. Esposito, R.; Anaç, C.; Hendriks, M.A.; Çopuroğlu, O. Influence of the Alkali-Silica Reaction on the Mechanical Degradation of Concrete. *J. Mater. Civ. Eng.* **2016**, *28*, 04016007. [CrossRef]
111. Li, Z.; Thomas, R.J.; Peethamparan, S. Alkali-silica reactivity of alkali-activated concrete subjected to ASTM C 1293 and 1567 alkali-silica reactivity tests. *Cem. Concr. Res.* **2019**, *123*, 105796. [CrossRef]
112. Beglarigale, A.; Yazici, H. Mitigation of Detrimental Effects of Alkali-Silica Reaction in Cement-Based Composites by Combination of Steel Microfibers and Ground-Granulated Blast-Furnace Slag. *J. Mater. Civ. Eng.* **2014**, *26*, 04014091. [CrossRef]